PHYSICS DESIGN OF THE NATIONAL SPHERICAL TORUS EXPERIMENT

PLASMA ENGINEERING

KEYWORDS: *experimental devices, National Spherical Torus Experiment, spherical tori*

STANLEY M. KAYE* and MASAYUKI ONO
Princeton Plasma Physics Laboratory, Princeton University
Princeton, New Jersey 08543

YUENG-KAY MARTIN PENG *Oak Ridge National Laboratory*
Oak Ridge, Tennessee 37830

DONALD B. BATCHELOR and MARK D. CARTER
Oak Ridge National Laboratory, Oak Ridge, Tennessee 37830

WONHO CHOE
Korea Advanced Institute of Science and Technology, Taejon, Korea

ROBERT GOLDSTON *Princeton Plasma Physics Laboratory*
Princeton University, Princeton, New Jersey 08543

YONG-SEOK HWANG
Korea Advanced Institute of Science and Technology, Taejon, Korea

E. FRED JAEGER *Oak Ridge National Laboratory*
Oak Ridge, Tennessee 37830

THOMAS R. JARBOE *University of Washington*
Seattle, Washington 98105

STEPHEN JARDIN, DAVID JOHNSON, ROBERT KAITA, CHARLES KESSEL, and HENRY KUGEL
Princeton Plasma Physics Laboratory, Princeton University
Princeton, New Jersey 08543

RAJESH MAINGI *Oak Ridge National Laboratory*
Oak Ridge, Tennessee 37830

RICHARD MAJESKI, JANHARDAN MANICKAM, JONATHAN MENARD, and DAVID R. MIKKELSEN
Princeton Plasma Physics Laboratory, Princeton University
Princeton, New Jersey 08543

DAVID J. ORVIS and BRIAN A. NELSON
University of Washington, Seattle, Washington 98105

FRANCO PAOLETTI *Columbia University*
Department of Applied Physics, New York, New York 10027

NEIL POMPHREY and GREGORY REWOLDT
Princeton Plasma Physics Laboratory, Princeton University
Princeton, New Jersey 08543

*E-mail: skaye@pppl.gov

STEVEN SABBAGH *Columbia University*
Department of Applied Physics, New York, New York 10027

DENNIS J. STRICKLER *Oak Ridge National Laboratory*
Oak Ridge, Tennessee 37830

EDMUND SYNAKOWSKI and JAMES R. WILSON
Princeton Plasma Physics Laboratory, Princeton University
Princeton, New Jersey 08543

Received August 25, 1998
Accepted for Publication November 24, 1998

The mission of the National Spherical Torus Experiment (NSTX) is to prove the principles of spherical torus physics by producing high-β_t plasmas that are noninductively sustained and whose current profiles are in steady state. The NSTX will be one of the first ultralow-aspect-ratio tori ($R/a \leq 1.3$) to operate at high power (P_{input} up to 11 MW) to produce high-β_t (25 to 40%), low-collisionality, high-bootstrap-fraction ($\leq$70%) discharges. Both radio-frequency and neutral beam heating and current drive will be employed. Built into the NSTX is sufficient configurational flexibility to study a range of operating space and the resulting dependences of the confinement, micro- and magnetohydrodynamic stability, and particle- and power-handling properties. NSTX research will be carried out by a nationally based science team.

I. INTRODUCTION

Spherical tori (ST) can potentially provide an attractive path to a reactor or volumetric neutron source (VNS). The ST fusion core would be small and economic with high-power density, and with the use of a copper toroidal field (TF) coil inner leg and without a large inboard shield and ohmic heating (OH) transformer, it would be a simple and reliable system. With encouraging experimental results from present low-aspect-ratio experiments, such as START (Ref. 1), CDX-U (Ref. 2), and the Helicity Injected Torus (HIT) (Ref. 3), and encouraging theoretical predictions,[4–6] the National Spherical Torus Experiment (NSTX) has been approved and is presently under construction. Various reactor concepts have been advanced for the ST (Refs. 7 and 8), and these have identified issues of importance in the development of ST-based fusion power. NSTX will address many of these issues, including transport and confinement, magnetohydrodynamic (MHD) stability, noninductive operation, and power and particle handling.

The overall goal of NSTX is to prove the principles of ST physics in a 1-MA device that can produce high-β_t plasmas in noninductively sustained discharges whose current profile is in steady state, with an aim toward creating a cost-effective pathway to a fusion core. It is the set of issues related to developing an attractive ST fusion core that forms the basis for the performance objectives of NSTX. The purpose of this paper is to present the physics basis for the design of NSTX, along with the hardware capabilities required to achieve these performance objectives and thus pave the way for continued development of the ST concept. The zero-dimensional (0-D) calculations that elucidate some of the key ST physics/fusion core issues will be presented in Sec. II, followed by a discussion of the resulting experimental objectives, baseline device capabilities, and the general physics basis for exploring the ST configuration in NSTX. Following this, the details of the physics calculations in the areas of configurational flexibility, confinement and transport, MHD stability and β_t limits, heating and current drive, and power and particle handling will be presented. Finally, there will be a brief discussion of the planned diagnostics and preliminary research plan.

II. SIMPLE 0-D CONSIDERATIONS

Some of the key advantages of the ST configuration, along with some of the issues, can be seen from simple 0-D considerations. We start from the definition of fusion yield:

$$P_{fusion} \simeq Vol \cdot (nT)^2 \cdot \frac{\langle \sigma v \rangle}{T^2} \simeq Vol \cdot B_0^4 \cdot \beta_t^2 \cdot \frac{\langle \sigma v \rangle}{T^2} \quad . \tag{1}$$

Here, and throughout the paper, β_t is defined as $2\mu_0 \langle p \rangle / B_0^2$, B_0 being the vacuum toroidal magnetic field at the geometric radius. The cost of a fusion core depends on the volume and the magnetic field; the fusion cross-section and plasma temperature are dependent on the plasma properties. One way to reduce the cost of a fusion core for fixed volume is to reduce the magnetic field B_0, which can be done if β_t is high enough.[6]

It is often convenient to express the stability limit for the plasma β_t as

$$\beta_t = \beta_n \frac{I_p}{aB_0} , \tag{2}$$

where I_p is plasma current, a is plasma minor radius, and β_n is a constant, which is typically two to four in conventional-aspect-ratio tokamaks. The advanced physics regimes have achieved or are predicted to attain a β_n of four to six. The MHD analyses of low-aspect-ratio tori have led to predicted values of β_n from four to greater than eight for optimized current and pressure profiles and with the presence of a nearby conducting shell.[4] It is clear from Eq. (2) that raising the plasma current increases β_t for a given β_n. The plasma current increases dramatically at fixed $q(a)$ as the aspect ratio is reduced, as can be seen from the relation

$$I_p \simeq \frac{1+\kappa^2}{2} \frac{R_0 B_0}{q(a)} \frac{Af(A)}{(A^2-1)^2} , \tag{3}$$

where

κ = elongation

R_0 = plasma major radius

$q(a)$ = inverse rotational transform at the plasma edge

$A = R_0/a$

$f(A) = 1.22A - 0.68$ (Ref. 9).

The increase in plasma current with decreasing A is mainly due to the field pitch behavior in the inner part of the torus near the center TF post. As A decreases, the magnetic pitch goes down as $(A^2-1)^2$ since the toroidal field increases and the toroidal circumference decreases while the poloidal magnetic field remains relatively unchanged. The inherent high-current nature of the ST plasmas has been demonstrated in the experiments on START (Ref. 10) and CDX-U (Ref. 2).

Higher-plasma current is also generally favorable for plasma confinement in strongly heated plasmas. As aspect ratio is reduced at fixed q, the resulting increase in plasma current improves confinement in present-day empirical scaling expressions.[11–13]

Incorporating Eqs. (2) and (3) into Eq. (1), one obtains

$$P_{fusion} \propto \beta_n^2 \kappa (1+\kappa^2)^2 \frac{R_0^3 B_0^4}{q(a)^2} \frac{A^2 f(A)^2}{(A^2-1)^4} , \tag{4}$$

which illustrates the parameters that most strongly influence the amount of fusion power produced. The fusion power can increase significantly as aspect ratio is reduced. It is also a strong function of plasma elongation.[6] It is well known that as the aspect ratio is reduced, the plasma elongates naturally without external coils.[9,14] This behavior is a consequence of the strong toroidicity of ST plasmas. The natural elongation is also a strong function of the plasma internal inductance, with κ increasing as l_i is reduced.[15] For ST fusion cores, where it can be quite difficult to create elongation by external coils, it is highly desirable to have this natural elongation to enhance the fusion yield.

Another consideration for fusion power yield is the maximum allowable magnetic field. In a toroidal device, the maximum magnetic field B_{max} usually occurs at the outer region of the inner leg of the TF coil, $R_c = R_0 - a - \Delta$. Here, Δ is the distance between the coil and the inner plasma edge. If the coil is a superconducting magnet, B_{max} is typically limited to ~13 T. The normal conductor magnetic field can be significantly higher. Since B_{max} is related to B_T by $B_{max} R_c = B_0 R_0$, the fusion power can be rewritten as

$$P_{fusion} \propto \beta_n^2 \kappa (1+\kappa^2)^2 \frac{R_0^3 B_{max}^4}{q(a)^2} \times \left[\frac{A - 1 - \Delta/a}{A^2 - 1} \right]^4 \frac{f(A)^2}{A^2} . \tag{5}$$

The gap size should be made as small as possible for maximizing fusion yield. Assuming the gap can be ignored, which is essentially the same as assuming there is no OH solenoid, the equation can be reduced to

$$P_{fusion} \propto \beta_n^2 \kappa (1+\kappa^2)^2 \frac{R_0^3 B_{max}^4}{q(a)^2} \frac{f(A)^2}{(A+1)^4 A^2} . \tag{6}$$

The fusion yield favors low aspect ratio both with and without a gap, although optimizing the fusion yield depends on consideration of all the parameters in the foregoing equation.

The final important factor for an ST fusion core that will be considered here is the ratio of fusion power to the resistive power used for the TF magnet. Clearly, it is desirable to minimize the recirculating fusion power. The TF coil resistive dissipation is concentrated in the TF center leg for ST devices. The parametric dependence of the coil resistance can be expressed as

$$P_{TF} \propto \kappa J_{TF}^2 R_0^3 \frac{(A - 1 - \Delta/a)^2}{A^2} \propto \kappa R_0 B_{max}^2 . \tag{7}$$

Therefore, the ratio of the fusion power to the power dissipated in the center leg is

$$\frac{P_{fusion}}{P_{TF}} \propto \beta_n^2 (1+\kappa^2)^2 \frac{R_0^2 B_{max}^2}{q(a)^2} \frac{f(A)^2}{(A+1)^4 A^2} . \tag{8}$$

As was found with Eq. (6), this ratio favors low A, although optimization of all the parameters is necessary for minimizing the recirculating power.

III. EXPERIMENTAL OBJECTIVES

The 0-D considerations presented in Sec. II illustrate some of the physics issues that must be addressed and performance objectives that must be achieved to advance the ST concept. It is clear that the low-aspect-ratio configuration must operate at high β_t, high plasma current, high elongation, and with little or no OH solenoid. To this end, the experimental and performance objectives that have been established for NSTX are as follows:

1. achievement of $\beta_n \geq 4$, $\beta_t \sim 25\%$ at low collisionality for first stability regime plasmas ($q_0 \sim 1.0$)
2. achievement of $\beta_n \geq 8$, $\beta_t \sim 40\%$ at low collisionality in advanced physics scenarios ($q_0 \sim 2.5$)
3. demonstration of noninductive discharge startup to current levels of 0.5 MA
4. demonstration of full noninductive, steady-state current sustainment with high bootstrap fraction (70%)
5. demonstration of adequate power and particle-handling capability at high β_t and long pulse length.

To achieve these objectives, the NSTX device was designed with the capabilities listed in Table I.

Achieving high β_t (25 to 40%) at low collisionality requires adequate confinement and auxiliary heating, and NSTX will be one of the first ultralow-aspect-ratio tori ($R/a \leq 1.3$) to operate at high power (P_{input} up to 11 MW). Performance estimates from neutral beam injection (NBI) discharges in START (Ref. 16) indicate good confinement at low aspect ratio. However, the parametric dependence of energy confinement at low aspect ratio is not yet known, and understanding the confinement scaling and transport physics at low aspect ratio with high heating power, low collisionality, and high density is one of the major elements of the NSTX mission. Suppression of electrostatic and electromagnetic microinstabilities due to increased orbit-averaged good curvature, as indicated by code calculations,[5] and the role of the high velocity shearing rate, due to the low toroidal magnetic field, will also be a focus of these confinement and transport studies.

Recent START results[1] have demonstrated the ability of STs to produce high β_t ($\beta_t \simeq 40\%$, $\beta_0 \simeq 100\%$) in the first stability regime ($q_0 \sim 1$). NSTX will investigate high-β_t ($\geq 25\%$) equilibria, specifically addressing the dependence of the ballooning and kink instabilities on variations in aspect ratio, shaping, and the presence of conducting plates. The presence of conducting plates is important for attaining high β_t; results from PBX and PBX-M (Refs. 17 and 18) indicate that passive conducting plates in close proximity to a rotating plasma can reduce the growth rates for low-n global MHD modes, thus enhancing the plasma stability and leading to higher β values. The conducting plates, however, must be able to withstand escaping heat and particle flux without compromising plasma purity.

High q, q_0 operation at low collisionality and high β_t lends itself to high bootstrap current regime investigations, while low q, q_0 operation will focus on studying the maximum β_t limits for stable, disruption-free operation.

For the high-performance plasmas, the β and the shaping factor S are typical of what would be required for an ST VNS or reactor. Results from DIII-D (Ref. 19) indicate that $\beta_t \tau_E$ is a strong function of the shaping parameter $S = I_p q_\psi / a B_T$. The shaping parameter can be written in the form $S = [A/(A-1)^2](1+\kappa^2)/2$, where the elongation κ increases strongly as $A \rightarrow 1$, a benefit of the naturally high elongation inherent in ST plasmas. For NSTX plasmas, S is expected to be ~80, which is more than a factor of 10 greater than that of present-day conventional-aspect-ratio tokamaks.

Another capability that is built into NSTX to enable it to achieve its objectives is configurational and shape flexibility. Flexible shape control is required to explore a wide range of plasma elongation and triangularity to optimize the plasma stability. Furthermore, it will be necessary to adjust the plasma shape and position to maximize the scrape-off layer (SOL) flux tube expansion under the constraints imposed by the fixed position of the conducting plates and by the required X-point position. The ability to control the plasma shape and position is important

TABLE I

Device Capabilities

R	0.85 m
a	0.68 m
I_p	1 MA
B_T	0.3 T
κ	2.0
R/a	1.25
Startup	OH, electron cyclotron heating (CHI)
Wall stabilization	Close-fitting conducting plates
Auxiliary heating and current drive	CHI, HHFW (6 MW), NBI (5 MW)
Profile control	HHFW, CHI, NBI
Maximum pulse length	5 s (> current relaxation time)
Divertor	Single- and double-null, IWL
Profile diagnostics	

for assessing the benefits of low aspect ratio in suppressing microinstabilities believed to be responsible for radial heat and particle transport. Finally, configurational flexibility is crucial to producing a range of divertor configurations; specifically, a single-null configuration is required for coaxial helicity injection[3] (CHI).

The current in an ST fusion core, which can be at levels of tens of megaamperes, must be produced and maintained noninductively since an ST reactor will not likely be able to support an OH capability due to space and power limitations. The development of noninductive startup techniques is therefore crucial to the ST development path. NSTX will, during its first phase of operation, employ CHI as the primary noninductive startup technique. CHI has been used successfully on the Helicity Injected Tokamak (HIT) to produce a 200-kA plasma,[3] and extrapolation to NSTX based on injector-current-to-plasma-current conversion efficiency indicates that producing a 500-kA plasma is possible. Since CHI is a technology that still needs development in ST plasmas, NSTX is designed with the capability to produce and to drive current inductively to ensure that other critical physics can be studied. Approximately 0.9 V-sec are available from the OH windings and poloidal field (PF) coil set, with about two-thirds of the total V-sec being produced by the OH. Inductive breakdown will be aided by 20 kW of electron cyclotron (EC) preionization. EC preionization may also be employed to aid CHI startup.

During the main phase of NSTX discharges, 6 MW of high harmonic fast waves (HHFW) and 5 MW of NBI will be the primary auxiliary heating and, along with bootstrap current, the primary noninductive current-drive techniques. At low-ion β, the HHFW will preferentially heat electrons.[20] This serves two purposes: The first is to drive current directly, and the second is to increase the bootstrap current fraction that is driven through the hotter electrons. HHFW will provide current profile control through $n_{\|}$ control during the flattop phase of the discharge, although at higher β_t, the HHFW current will be driven off-axis. Alternatively, NBI-driven current will be peaked on-axis for the expected plasma densities and beam orientation.

The possibility of driving current during the current sustainment phase in the very outer portion of the plasma with CHI will be explored. As will be seen in a later section, some edge current drive ($\sim$25%) is required for producing the necessary profiles for the highest-β_t target.

These different current-drive and heating techniques provide the capability for current and pressure profile control and, thus, the ability to explore a wide range of operational scenarios to both study fundamental ST physics as well as produce high-performance ST plasmas.

It is important that the evaluation of the confinement and MHD properties of ST discharges be in a steady-state regime, where the current profiles have had adequate time to fully relax, to assess the reactor potential for stable, high-β_t scenarios. Typical 1-MA current flattop durations for inductive operation of NSTX with auxiliary heating range from 150 ms to 0.5 s, generally depending on the type of heating employed (ion heating with NBI or electron heating with HHFW). A 0.5-MA CHI target plasma would greatly increase the current flattop duration due to savings in inductive V-sec. While the inductive operation pulse lengths may be five to ten times the plasma energy confinement time, the 0.5-s current flattop duration is not long enough for the current profile to attain steady state. Estimates based on the results of a current relaxation study[21] indicate that the time constant for the current profile to relax for typical NSTX parameters is from 1 to 2 s for the constant current and voltage boundary conditions, conditions which would be expected during the current sustainment phase of the discharge. Consequently, because the required current relaxation time constant is longer than the inductive current flattop duration, noninductive current drive is an essential ingredient also in attaining a current profile in steady state. Furthermore, NSTX was designed for pulse lengths up to 5 s for this noninductive operation, the pulse length limited to this duration by the heating of the center stack TF coil.

Divertor heat loads in STs are expected to be high because of the compact nature of this configuration. The divertor and limiter surfaces in NSTX must be able to handle the power densities produced in the high-β_t, long-pulse discharges with the initial 6 MW of radio-frequency (rf) heating along with a heating system upgrade to 11 MW (with NBI). Estimates indicate that the baseline 6 MW of heating may result in power densities on the divertor plate of the order 15 MW/m^2. The vacuum vessel volume must be adequate to allow plasma configurations that maximize the range of SOL flux tube expansion, which is estimated to be up to a factor of 4. Inertial cooling of the divertor plates, as well as the plasma-facing components on other limiting surfaces, is generally adequate for 5-s pulse lengths, although at the highest power densities, either the pulse lengths will have to be shorter than 5 s and/or divertor sweeping will be employed. The machine design can accommodate a divertor cryopump as an upgrade possibility.

Finally, much emphasis will be placed on detailed diagnosis of the plasma characteristics, with specific aims of determining and understanding the MHD stability (including disruption mechanisms), transport and microinstabilities, and divertor characteristics.

In the remainder of this paper, we will present the details of the physics calculations in the areas mentioned earlier, and this will be followed by a brief discussion of the planned diagnostics and preliminary research plan.

IV. REFERENCE GEOMETRY

A cross section of NSTX is shown in Fig. 1. Some of the notable features to point out include the close-fitting

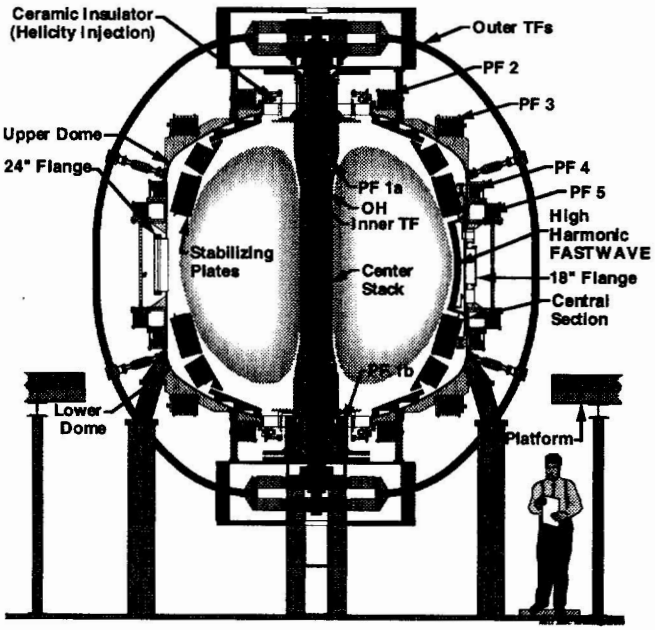

Fig. 1. NSTX cross section.

conducting plates, whose purpose is to slow down or stabilize the plasma vertical motion and growth of low-n instabilities, the divertor region, including a slot between the upper conducting plate and outer divertor plate for possible future cryopumping, the set of PF coils, and ceramic breaks for isolating vessel segments for CHI. The set of PF coils includes five up-down symmetric pairs (PF1a and PF2 through PF5) and one coil, PF1b, which is only in the lower half-plane. PF1b will be used specifically for controlling the X-point and separatrix leg positions in single-null discharges for CHI. It is important for the success of CHI to have one separatrix leg on each of the CHI electrodes; each divertor plate on either side of the ceramic break and the PF1b coil constitute an electrode.

PF3 and PF5 will provide the vertical field necessary for radial control of the plasma, while PF1a, PF2, and also PF3 will be used for controlling the plasma shape. During the initial operation of the device, PF4 will not be used; this coil will be used at a later date to enhance the shape control capability of the device. Table II lists the number of turns in the OH and in each PF coil (in each half-plane) and the coil current/turn limit (absolute value) for each. The power supplies associated with each PF coil do not limit the achievable coil current. It is also noted that a more than sufficient number of power supplies exist so that each coil can be controlled separately (i.e., upper and lower) and can have bipolar capability if necessary.

To study the uncharted region of ST physics, a great deal of configurational flexibility has been built into NSTX. This flexibility, which includes different plasma

TABLE II

OH and PF Coil Capabilities

Coil	Number of Turns	Coil Current/ Turn Limit (kA)
OH	482	24
PF1a	48	15
PF1b	32	20
PF2	28	20
PF3	30	20
PF4	17	20
PF5	24	20

shapes at fixed-aspect-ratio as well as different-aspect-ratio configurations, will allow exploration of transport characteristics and MHD stability boundaries, and it will also allow for some optimization of the power-handling capability and rf coupling. The coil currents necessary for producing the different plasma configurations at fixed aspect ratio are not restricted by coil or power supply limitations. As an example, Fig. 2 shows three reference configurations: inner wall limited (IWL), double-null X point, and single-null X point. The single-null X-point configuration, as noted in Sec. III, is necessary for CHI. For the NSTX configurations, the vertical field is provided mainly by PF3 and PF5, two of the outermost coil sets, while shaping is controlled primarily by the two inner coils, PF1a and PF2. In the IWL configuration, only PF3 is needed in addition to PF5. For the diverted configurations, both PF1a and PF3 are needed to move the X point into the region inside the vacuum vessel. PF1b is needed for fine-tuning the position of the X point and separatrix legs in the single-null configuration for CHI.

The range of accessible elongation and triangularity has been computed and is shown in Fig. 3. In this calculation, both first stability ($q_0 \sim 1.0$) and advanced physics regime ($q_0 \sim 2.5$) configurations were considered. From the figure, it can be seen that a range of shapes can be produced. This capability allows the exploration of the dependence of MHD stability and confinement on these parameters. The flexibility also allows for the adjustment of shapes for ameliorating high-heat fluxes on the divertor plates. The results shown here used only the coil current and power supply limits as constraints, with no consideration given toward MHD stability properties. It is to be noted that while the entire range of shapes can be produced within the power supply and coil current limits, these limits are challenged for PF2 and PF3 for low-elongation and low-triangularity double-null plasmas. The reason for this is the high natural elongation of ST plasmas. For NSTX, the natural elongation is >2 at the low l_i values ($\leq$0.6) expected to be produced. To reduce the elongation to values near 1.6 requires sufficient current

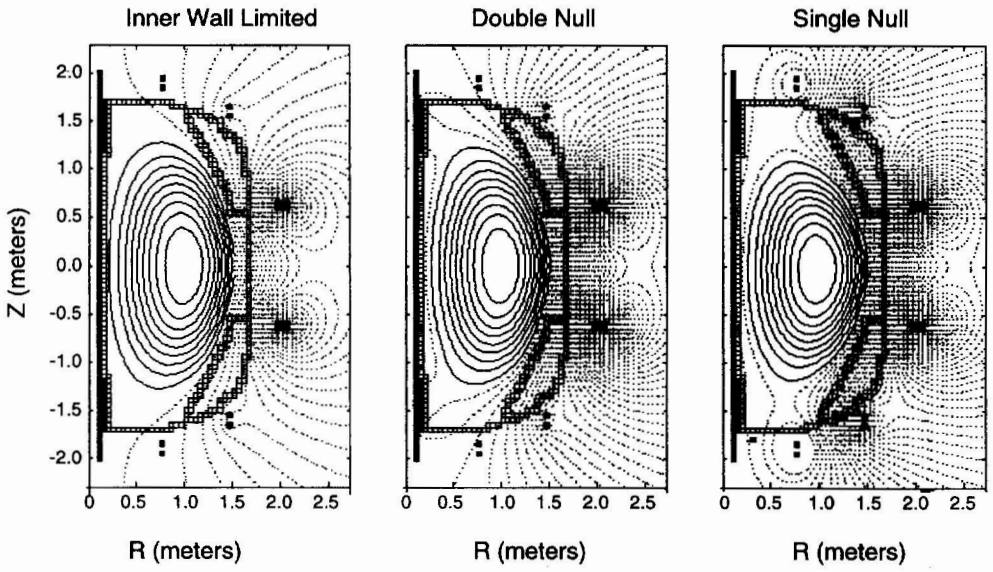

Fig. 2. NSTX configurations.

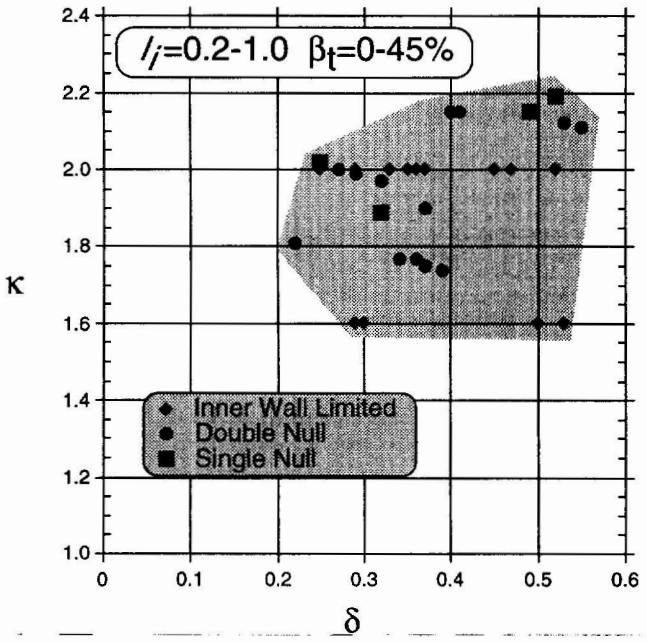

Fig. 3. NSTX shape flexibility for IWL and double- and single-null configurations.

in PF2 and PF3 to counteract this natural elongation, and the required currents in these coils can be close to the mentioned limits. This is not the case for the IWL plasmas. It is also possible to produce IWL plasmas with $A = 1.4$ and $\kappa = 3$. However, these plasmas, with $R = 0.7$ m and $a = 0.5$ m, would be too far from the conducting plates to gain the benefit of the enhanced vertical and MHD stability that the plates provide.

NSTX is also capable of producing plasmas with varying aspect ratios, from the nominal value near 1.25 up to 2.0, all within the coil capabilities of the device. This is important for the MHD stability and confinement studies, not only because of the direct connection that can be made with the conventional, higher-aspect-ratio database, but because of the expectation that microinstabilities are expected to be suppressed with decreasing aspect ratio, and the ability to scan in R/a will facilitate the direct study of this effect.

V. PHYSICS FOCUS AREAS

V.A. Confinement and Transport

One of the primary mission elements of NSTX is to determine the confinement scaling at low aspect ratio and make a connection between this scaling and those at the higher, more conventional aspect ratio for which a multitude of global confinement scalings have been developed. The only information about confinement behavior at low R/a with auxiliary heating comes from START (Ref. 1). START operated with NBI whose powers ranged up to ~0.8 MW. These power levels were comparable to the OH heating-power levels. START plasmas exhibited characteristics of H-mode plasmas: increase in line-averaged density, flat density profiles with steep edge density gradients, and edge-localized mode (ELM)-like behavior. The deduced confinement times agreed well with one to two times some popular L-mode scalings, most notably the Lackner-Gottardi-Connor scaling (Lackner-Gottardi with a low-aspect-ratio correction made by Connor).[22,23] This scaling has parametric

dependences generally similar to those of the International Thermonuclear Experimental Reactor (ITER) 89-P (Ref. 11), but with a stronger size and density dependence.

The H mode should be easily attainable in NSTX, based on the predictions of various L- to H-mode scaling expressions. While no one expression has been accepted as the standard for determining the threshold power, several expressions do a reasonably good job in describing the lower threshold boundary for "easy transition" discharges.[24] Using the baseline NSTX parameters, these expressions give a range for the threshold power level from tens to 150 kW, indicating that the H mode should be accessible in NSTX plasmas, which will be heated at the multimegawatt power levels.

As discussed in Sec. III, the NSTX performance goals include achieving β_t (β_n) values of ~25% (4) for first stability regime plasmas and up to 40% (8) in advanced regimes. Estimates of the power required to attain these values are shown in Fig. 4. Plotted in the figure is the achievable β_t (β_n) as a function of heating power for confinement enhancements of 1, 2, and 3 relative to the ITER97L scaling.[13] This is a recently developed L-mode scaling, which has parametric dependences similar to those of ITER89P but which is ~10% more pessimistic (i.e., lower confinement times) than ITER89-P and ~70% more pessimistic than Lackner-Gottardi-Connor for the NSTX baseline parameters. An enhancement factor of 2.0 applied to ITER97L gives the same confinement time as applying an enhancement factor of ~1.2 to Lackner-Gottardi-Connor (which for NSTX baseline parameters is ~40 ms). What is seen from the figure is that the high-β target is accessible with ~4 to 5 MW of heating power at the highest enhancement factor but that ~11 MW of power is needed to achieve this target at H = 2. The highest β_t values are not accessible for H = 1 using this confinement expression. At high β_t, the "volume averaged" electron collisionality ($\propto\langle n_e\rangle/\langle T_e\rangle^2$) is comparable to what would be expected in an ST fusion core.

The ability to produce low-collisionality plasmas with strong auxiliary heating, as well as the ability to operate over a range of aspect ratios, allows NSTX to explore the benefit of low aspect ratio in suppressing both electrostatic and electromagnetic transport-inducing microinstabilities. The expected behavior of these instabilities was studied using a comprehensive kinetic toroidal microinstability code, which takes into account high-n effects, all resonances, finite β, finite-Larmor radius, and banana orbit effects.[5] The study was performed for plasmas at fixed $q_* [\equiv q_{cyl}(1+\kappa^2)/2]$ and RB_T, over a range of aspect ratio from 1.25 to 2.5. The results show that both the kinetic ballooning mode (electromagnetic) and the trapped electron-η_i mode (electrostatic) are suppressed as the aspect ratio is lowered. The growth rates are plotted as functions of aspect ratio for both modes at the $\Psi = 0.7$ flux surface in Fig. 5. The "n" numbers for the electromagnetic mode are the toroidal mode

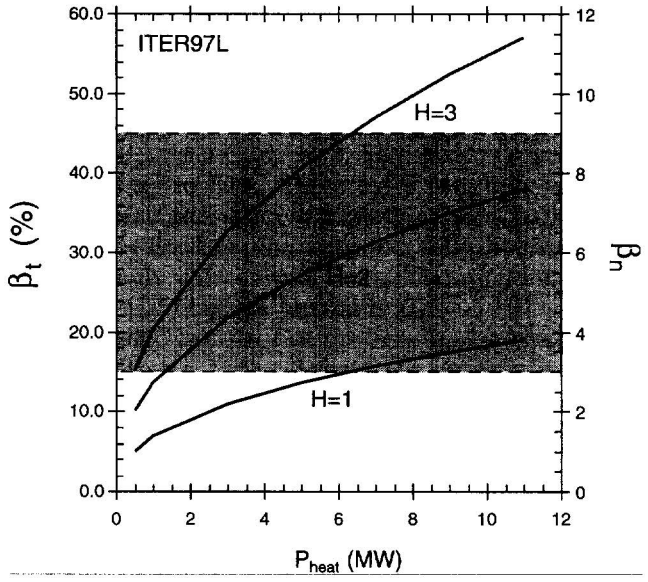

Fig. 4. Achievable β_t, β_n as functions of auxiliary heating power for three different enhancement factors relative to ITER97L scaling.

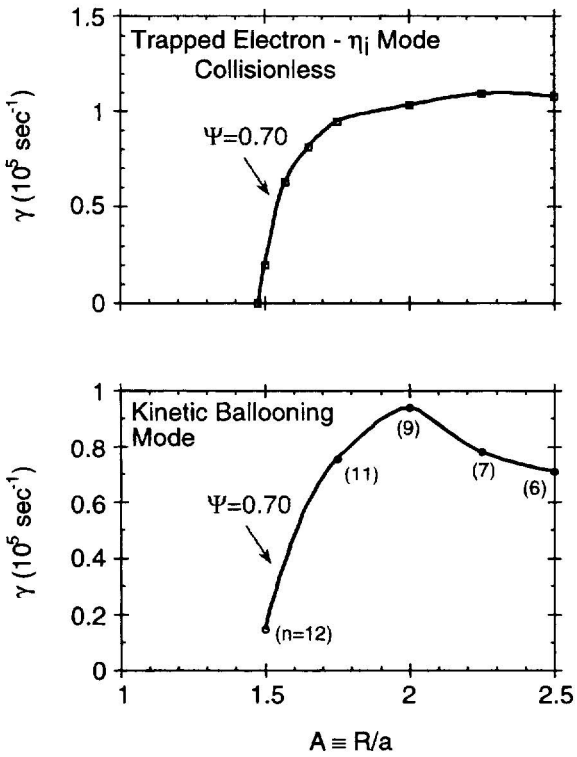

Fig. 5. Growth rates as functions of aspect ratio for electromagnetic and electrostatic modes.

numbers of the most unstable mode on that surface. As can be seen, the growth rates start to decrease sharply at $R/a \sim 1.5$, with complete stabilization of these modes on this flux surface at $R/a \simeq 1.3$ to 1.5. The reason for stabilization of these modes with decreasing aspect ratio can be linked to the strong toroidicity of these plasmas, which leads to a reduction in the orbit-averaged bad curvature (the instability drive).

In addition to the effect of reduced orbit-averaged bad curvature, the low toroidal field of NSTX is an advantage with respect to flow shear for stabilization of microturbulence. Because the toroidal field is approximately one order of magnitude lower than that at conventional aspect ratio, the damping due to sheared flow will be strong. The shearing rate due to $E \times B$ flows is given by

$$\gamma_{E\times B} = \frac{RB_\theta}{B}\frac{d}{dR}\left(\frac{E_r}{RB_\theta}\right) , \qquad (9)$$

where the E_r is composed, primarily, of one term proportional to the plasma pressure gradient and one term proportional to the toroidal flow.[25] Both terms can be important in NSTX. Figure 6 shows the shearing rate for NSTX, assuming broad pressure profiles optimized for MHD stability (see Sec. V.B) and different toroidal flow Mach numbers. The influence of the toroidal flow can be seen by the difference in shearing rates at different Mach numbers. The shearing rates themselves in the outer portion of the plasma ($R \geq 1.1$ m) can be up to an order of magnitude higher than the growth rates shown in Fig. 5. Turbulence suppression occurs for $\gamma_{E\times B} \geq \gamma_{mode}$. It is also seen that the shearing rate with a Tokamak Fusion Test Reactor (TFTR)-magnitude toroidal field is at least an order of magnitude lower than that in NSTX for the same Mach number.

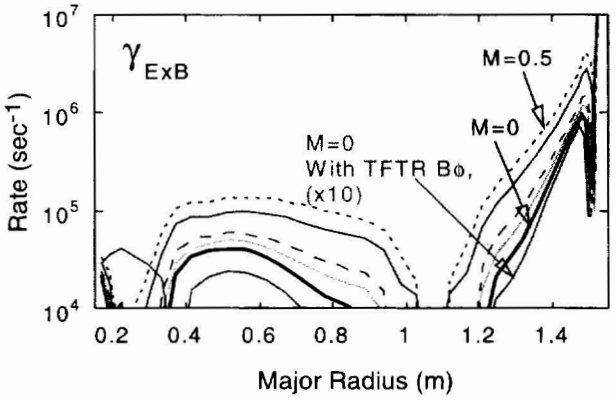

Fig. 6. NSTX $E \times B$ shearing-rate profile for different Mach numbers. Also shown for comparison is the shearing-rate profile for TFTR ($\times$ 10).

V.B. Stability and β Limits

Results on the axisymmetric and MHD stability properties of NSTX will be presented in this section.

The same self-fields that provide the natural elongation in ST plasmas through their vertical component provide a radial component that acts to slow down the ST plasma's vertical motion, thus enhancing its axisymmetric stability properties relative to those at conventional aspect ratio. Calculations were carried out using the TSC and TEQ codes to examine the vertical motion growth times in NSTX. The growth time is simply the inverse of the growth rate of the vertical instability. For these calculations, realistic models of the vacuum vessel, conducting plates, and connectors were used. With the conducting plates in place, the growth times for nominal NSTX plasmas with $l_i = 0.6$, $\kappa = 2.0$, and $\beta_t = 16\%$ is quite long, between 250 and 300 ms with the plates in place. For comparison, the vertical motion growth time for this plasma without the plates is of the order of milliseconds, which is still considerably longer than that at conventional aspect ratio. The growth time (with the plates) is not a strong function of β, remaining approximately constant as β_t is raised to 40% and decreasing to ~100 ms as β_t is lowered to a few percent. A larger variation is seen as a function of l_i, however. Figure 7 shows the vertical growth time as a function of l_i for double-null plasmas with $\beta_t = 13\%$. As can be seen, the maximum growth time occurs near $l_i = 0.5$, and it decreases to 0.12 s at

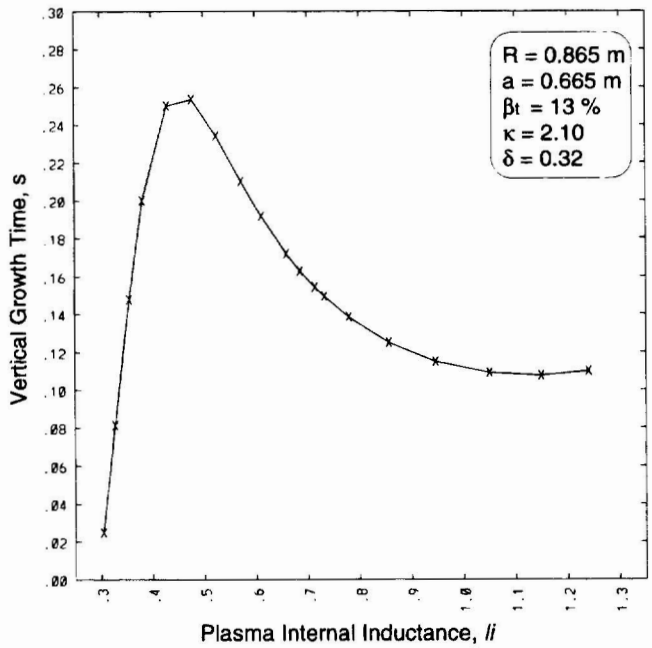

Fig. 7. Vertical motion growth times as a function of l_i for an NSTX plasma with $\beta_t = 13\%$.

l_i = 1.0 due to an increase in the effective distance between the conducting plates and the current centroid as the current profile becomes more peaked. The vertical growth time also decreases dramatically by an order of magnitude as l_i is lowered toward 0.3. This reduction is due to the nonrigid motion and strong deformability of plasmas at low l_i with discrete passive stabilizers.[26,27]

For a compact spherical torus reactor to be attractive, it must operate at high β_t, with β_t values typically ≥30%. Because of this, MHD stability is a key issue at low aspect ratio. This discussion of MHD stability issues in NSTX will just highlight a more detailed discussion that is presented in Ref. 4.

Previous MHD stability studies at higher aspect ratio have identified the importance of certain dimensionless parameters that are useful in predicting MHD stability. The two most widely recognized are $q_* = (2\pi a)^2 B_0(1 + \kappa^2)/(2\mu_0 R_0 I_p)$ and the normalized beta, $\beta_n = \beta_t a B_0/I_p$. In general, kink modes limit the amount of plasma current, thus setting a lower limit on q_*. Pressure-driven modes, such as high-n ballooning modes, intermediate-n internal modes, and low-n kink modes, tend to limit the plasma pressure that can be contained with a given external magnetic field. At high aspect ratio, the β_n limit is three to four for first stability regime plasmas and five to six in the advanced physics (or second stability) regime.

A series of numerical scans were performed to determine the possible range of stable equilibria in NSTX-like plasmas (R/a = 1.2 to 1.45, κ = 1.6 to 2.2) (Ref. 4). The stability of the equilibria was determined using the PEST-II code for low-n kink stability and the BALLOON code for high-n stability. Three distinct regimes were noted. The first is operation at high β_t (β_n = 5 to 6) and low q_* (≤2). This regime typically is at low $\epsilon\beta_{pol}$ (≈0.5) and, therefore, has a low bootstrap fraction (≈40%). Equilibria in this regime require substantial current drive and therefore would not be suitable for a self-sustaining fusion core. A second regime with higher β_t and bootstrap fraction exists, in which $q_0 > 2$, $\epsilon\beta_{pol} \simeq 1.0$, $\beta_n \simeq 8$, and there is a bootstrap fraction of up to 80%. These cases rely only on edge current drive to suppress edge-localized ballooning modes. The third regime is nearly fully bootstrapped, requiring only core current drive. These plasmas have high $\epsilon\beta_{pol}$ (1.5) but are limited in β_t.

In detailed calculations, the benefit of low aspect ratio is clearly seen. Figure 8 shows the results of a scan in aspect ratio for a conventional, first stability regime, configuration (q_0 = 1.1) with a broad pressure profile ($p_0/\langle p\rangle$ = 1.8), at κ = 1.6, which is an elongation that is slightly less than the baseline design case of 2.0. Marginal stability points are shown for a case with q_*/q_0 = 1.5 and q_0 = 1.1. For aspect ratios other than 1.2, the conformal wall is at r_{wall}/a = 1.4. At R/a = 1.2, the wall is at r_{wall}/a = 1.2. The results show a marked increase in achievable β_n as aspect ratio decreases, especially for the low-n modes. The effect of the wall is also seen, as the marginally stable β_n increases significantly, especially for the n = 1 mode. In these conventional cases, however, it is the $n = \infty$ ballooning mode that sets the upper limit on achievable β_n at low R/a.

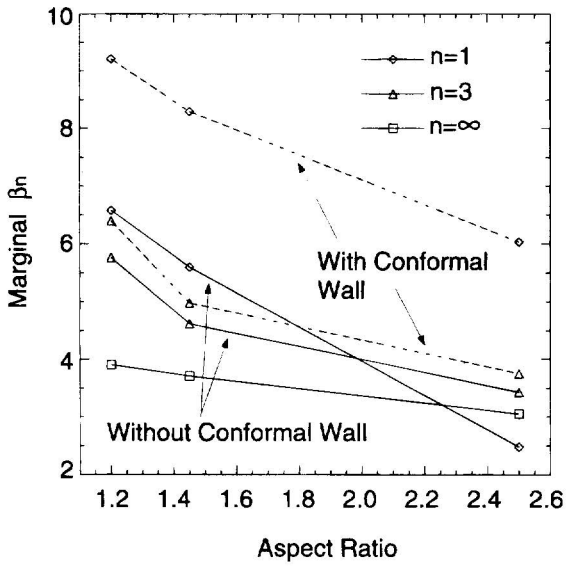

Fig. 8. Marginally stable β_n for kink and ballooning modes as a function of aspect ratio for q^*/q_0 = 1.5, q_0 = 1.1 (first stability regime). Solid lines indicate no conducting wall; dotted lines indicate a conformal wall. The $n = \infty$ (ballooning) mode, which is not influenced by the conducting wall, limits the β_n to ≤4 in these unoptimized cases.

The results of a calculation showing the marginal β values for a fully optimized equilibrium are shown in Fig. 9. For this equilibrium, q_0 = 2.83, q_*/q_0 = 0.69, and the actual locations and extent of the conducting plates were used. Both the β and bootstrap fraction were optimized for this target plasma. It is seen in the figure that for this case, the overall β limit is set by the n = 1 mode, to a value of 41.5% (β_n = 8.2). Higher-n modes show higher β limits, with the limit decreasing to ~43% ($\beta_n \sim$ 8.6) for the infinite-n ballooning mode. There is also a current-driven n = 1 mode whose stability depends on the edge q value, with $q(a)$ just above an integer being the most stable [here, $q(a)$ = 12.1]. The n = 2 to 5 kink modes do not appear to show this q dependence, and they have stability limits determined by pressure alone. For this optimized case, the total ∇p-driven current fraction is just over 70%.

The optimized equilibrium and profiles are shown in Fig. 10. The pressure profiles (c) for this optimized equilibrium are relatively broad, and the q profile (b) remains monotonic despite the hollow total current density profile (d). It can be seen from the panel showing the current profiles that for this equilibrium, the 30% of the current not carried by the bootstrap current, denoted "CD"

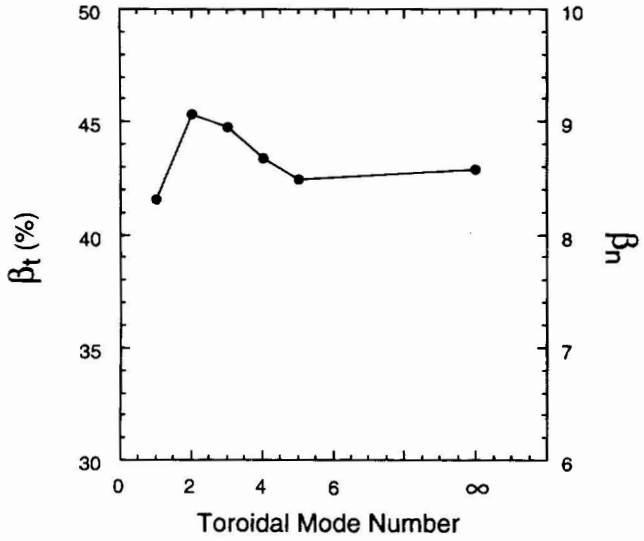

Fig. 9. Achievable β_t, β_n as functions of toroidal mode number for optimized pressure and current profiles.

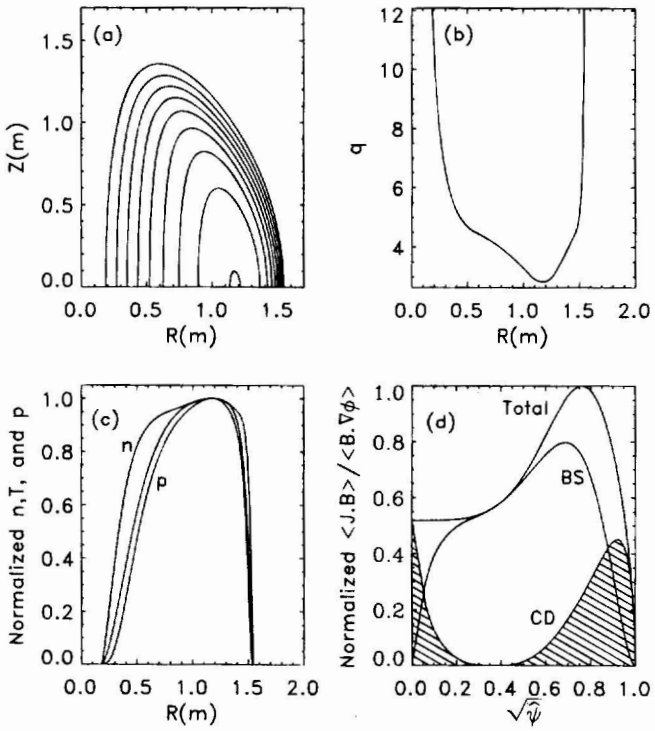

Fig. 10. Equilibrium and optimized profiles for the high-β target plasma. Shown are the (a) plasma equilibrium, (b) q-profile, (c) normalized density, temperature, and pressure profiles, and (d) current profile. The curves labeled BS and CD correspond to the bootstrap current profile and the current driven by external sources, respectively; $\hat{\psi}$ is the normalized poloidal flux.

in the figure, must be driven primarily in the outer region of the plasma. In actual operation, both CHI and HHFW will be used in an attempt to drive current in this location to sustain the mega-amperes fully noninductively.

One of the issues for effective passive stabilization is plasma rotation. This area is presently being studied for application to NSTX. One possibility is the natural rotation induced by rf current drive,[28] while another is the electromagnetic torque induced by appropriate phasing of a toroidal array of magnetic coils.[29] A tested method for inducing plasma rotation is through NBI, a system that is planned to be operational within 2 yr of first plasma.

V.C. Heating and Current Drive

An ST reactor design precludes an OH solenoid for two essential reasons. The first is that the center stack must be made as thin as possible because the inboard gap has such strong leverage in ST reactor economics, as shown in Sec. II. The second is the neutron damage on insulating materials that would inevitably occur. In addition to these, a compact ST reactor requires a high, steady-state current, typically 20 to 30 MA. These reasons make noninductive current drive an essential element of an ST reactor. The noninductive current drive can come from various sources: rf, neutral beams (NBs), and bootstrap current are the proven means. The bootstrap current, which can account for up to 75% of the total current in NSTX discharges, was discussed in Sec. V.B. The rf current drive can be considered after first noting the plasma dielectric constant $\omega_{pe}^2/\omega_{ce}^2 \gg 1$ for low aspect ratio. In fact, for typical NSTX parameters, this value is ~45. At this value, both lower hybrid and electron cyclotron waves have severe accessibility problems.

High harmonic fast waves are a promising alternative for heating and current drive at low aspect ratio. HHFWs show strong single-pass absorption for high-β operation, consistent with the high-density, low-toroidal-field regime of NSTX. HHFWs have good accessibility and will damp primarily on the electrons. At high ion β values, ion absorption can become important. The advantage of HHFW is that the electron heating can enhance bootstrap fractions, and the power deposition can be localized to some extent for profile control. Operation of HHFW on NSTX will nominally be at 30 MHZ (15th harmonic), and it will employ a 12-strap antenna situated at the midplane. Ultimately, 6 MW of rf power will be delivered.

It is necessary to deliver this high power over a range of plasma conditions, for not only will the HHFW be used to heat the plasma and drive current during the high-β sustainment phase of the discharge, but it will be necessary to heat the target OH plasma when β and the temperatures are relatively low. The RANT (Ref. 30) and PICES (Ref. 31) codes were used to study the coupling and deposition of HHFW power into various NSTX plasma equilibria. The HHFW current drive profiles were

estimated using the Ehst and Karney formulation[32] with trapped electron effects.

The calculation results show that the most promising regime for current profile control appears to be in the $\beta_t = 15\%$ range, with the 6 MW of rf driving up to 0.4 MA of current. Figure 11 shows the results of the calculations for $\beta_t = 5$ and 25% equilibria for various antenna phasings. In the 5% case [$T_i(0) = T_e(0) = 1$ keV], penetration to the core is good for all phasings, although there is not full single-pass absorption. Nevertheless, the results indicate that the HHFW will be effective in heating the plasma and driving up to 0.4 MA of current during this phase. For the 25% case, the single-pass absorption is good, with the power being deposited off-axis, as can be seen in the figure. Up to 0.3 MA of current is driven in this scenario for the 30- and 60-deg phasings. The current drive for the 90-deg phasing case is poor (0.1 MA) due to the slow phase velocity of the wave and the deposition profile being farther off-axis, which puts the wave power into the trapped electrons.

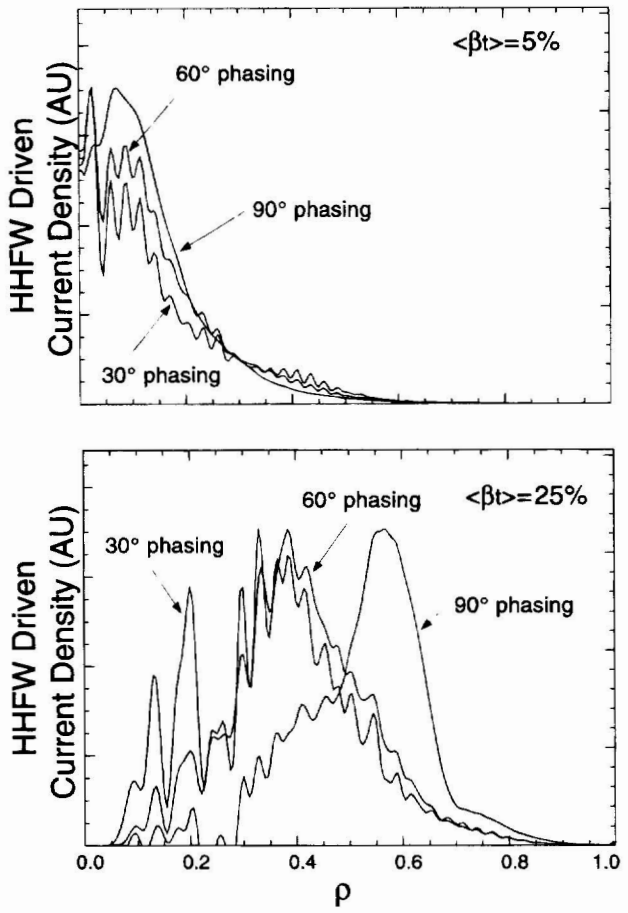

Fig. 11. Current density profiles driven by the HHFW for different antenna phasing and plasma β values; ρ is the square root of the normalized toroidal flux.

Neutral beam heating and current drive has been estimated for 5 MW of near-tangential injection into nominal NSTX equilibria ($\beta_t = 25\%$). The estimates are based on TRANSP calculations, which use a full-orbit Monte Carlo package to compute the NB deposition. TRANSP does this calculation in a self-consistent fashion, computing the internal equilibrium as well. The beam that will be used for NSTX is the spare TFTR neutral beam, consisting of three sources of deuterium at 80 kev, with the central source being injected at a tangency radius of 0.7 m and the two adjoining sources at ±0.1 m. The calculation indicates that only a few hundred kilowatts of heating power will be lost through shine-through, charge-exchange, or bad orbits for coinjection, so that most of the heating power will be available for this scenario. About 35% of the heating power is lost for counterinjection, primarily through bad orbits.

In the coinjection scenario, ~50% of the fast ions are on trapped orbits. The remaining passing particles impart enough momentum to electrons to drive ~0.2 MA of current. While the 0.2 MA is not enough to sustain the 1 MA current fully noninductively, it can play an important role in conjunction with other current drive techniques and bootstrap current. Both the heating and current drive profiles for NBI are peaked on-axis.

Coaxial helicity injection will be used to aid plasma startup and potentially to help sustain the full 1-MA current by current drive in the outer region. CHI delivers poloidal flux to the plasma edge through the use of biased electrodes, and this flux (toroidal current) is transported throughout the plasma via global MHD fluctuations. Approximately 0.2 MA of plasma current has been driven in HIT with CHI (Ref. 3) with a 10% conversion efficiency (injector current/driven current) at temperatures of ≈100 eV. From a physics perspective, NSTX provides an excellent 1-MA testbed for CHI at low aspect ratio. As discussed earlier in this section, it is expected that other noninductive current drive schemes in NSTX can provide up to 70% of the full current. It would therefore be necessary for CHI to provide ~0.30 MA of current during the flattop phase of the discharge for fully noninductive current sustainment and ~0.5 MA of current during startup. Given the available hardware, assuming the same 10% conversion efficiency, and given the larger size of NSTX relative to HIT, these levels of driven current should be available.[8]

V.D. Reference Discharge Scenarios and Plasma Performance

Details of simulations of reference discharge scenarios, including possible plasma performance and current flattop duration over a wide range of heating scenarios will be discussed in this section. The Tokamak Simulation Code (TSC) was used for these simulations. TSC is a time-dependent, free-boundary, predictive equilibrium and transport code whose strength lies in its ability to aid

in the scenario development of both discharge energetics and plasma control systems. TSC solves the fully dynamic MHD/Maxwell's equations coupled to transport and Ohm's law equations. TSC requires as input the device hardware and complement of coils and their respective electrical characteristics, assumptions concerning the plasma density profile (or a particle diffusivity), impurities, global discharge characteristics, PF coil currents, and position control feedback requirements. A more complete description of the code can be found in Refs. 33 and 34. TSC is not used to model plasma breakdown; these calculations, done using other codes, indicated the adequacy of the PF coils and associated power supplies for creating the field nulls necessary for inductive-only plasma initiation. The minimum stray field requirements are expected to be mitigated with the planned use of EC preionization.

TSC simulations were carried out for OH, rf, and NB-heated scenarios. For all these simulations, the multiplier of the plasma energy diffusivity, which is based on the Tang et al. model,[35] was adjusted to give a global confinement time comparable to the Lackner-Gottardi-Connor L-mode value, consistent with recent START NB-heating results. A typical reference discharge for an rf-heated inductive scenario is shown in Fig. 12. In this simulation, the current was initiated at time = 0 at a value of 20 kA, and then, under a current feedback control scheme, it was ramped inductively at a rate of 5 MA/s to the full 1 MA and then held at that level. Six MW of HHFW heating was turned on at 0.1 s, with the heating producing a central electron temperature of ~4 keV at a line-averaged density of 3.7×10^{19} m^{-3}. The density profile was assumed to be broad and given by

$$n(\psi, t) \propto n_0(t)\left[1 - \left(\frac{\psi - \psi_{min}}{\psi_{lim} - \psi_{min}}\right)^6\right]^{0.5} . \qquad (10)$$

The rf deposition profile was input into the calculation, and it was taken to be peaked on-axis during the initial phase of rf heating (0.09 to 0.2 s), and then it was taken to be peaked off-axis thereafter, consistent with the modeling results from the RANT and PICES codes (see Sec. V.C on heating and current drive). For this and other inductive discharge simulations reported here, no rf-current drive was assumed, although the calculated bootstrap current drive, amounting to ≈300 kA by the end of the flattop phase, was included. The omission of the rf-current drive leads to a conservative estimate of the possible current flattop duration.

In the bottom of the figure is the OH solenoid current necessary to produce the preprogrammed plasma current as a function of time. The OH current started at approximately +24 kA/turn and then decreased in time to its minimum value of approximately −22 kA/turn, at which point a total of ~0.9 V·s of flux has been produced (two-thirds of this by the OH). At this time, the 1-MA current has been sustained for ~0.5 s, giving a total pulse length, including the current rampup time, of 0.7 s. The plasma current is then ramped down over the next 0.4 s.

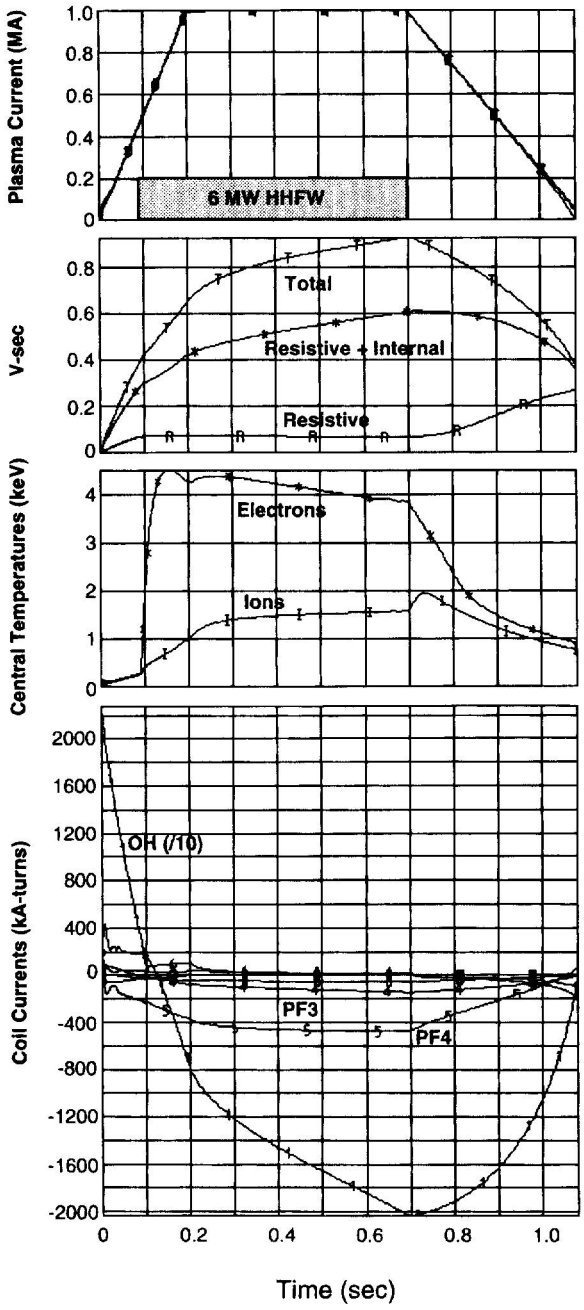

Fig. 12. Inductive reference discharge with HHFW heating.

The scenario shown in Fig. 12 was just one of the scenarios studied. Also simulated were scenarios with different plasma-current ramp rates and different heating scenarios. The change in rate of V-sec consumption from slowing the plasma current rampup rate down by over a factor of 2 did not change the ultimate flattop duration much. For rf-heated discharges, the flattop duration

remained in the 0.4- to 0.5-s range. With NBI instead of rf heating, the current flattop duration decreased to ~0.15 s, owing to a larger rate of V-sec consumption, both resistive (colder electrons) and inductive. There is virtually no current flattop duration at 1 MA for OH-only heated plasmas; 1 MA can be attained but not sustained. However, current flattop durations up to 0.5 s can be achieved in OH plasmas at maximum current levels of 0.5 MA, and over 1-s flattops can be achieved at 0.25 MA. A histogram showing the expected current flattop durations for the 1-MA current level is shown in Fig. 13.

The length of the current flattop duration can be enhanced greatly by using the CHI to produce a 0.5-MA target plasma noninductively and then using inductive means to ramp the current to the 1-MA level and sustaining it there. This is simply the result of not having to use V-sec to ramp the current to 0.5 MA inductively; therefore, the resulting V-sec savings can be used to extend the current flattop duration. It is seen in Fig. 14 that the V-sec savings results in 1-MA flattops ranging from several hundred milliseconds for OH to >1 s with HHFW heating.

NBI heats the ions preferentially, while the HHFW heats electrons preferentially. For the transport assumptions and heating profiles used in the simulations, the expected plasma densities and temperatures are given in Table III, indicating multikilo-electron-volt temperatures for both species in either auxiliary heating scenario. The NB deposition profile was input to TSC but

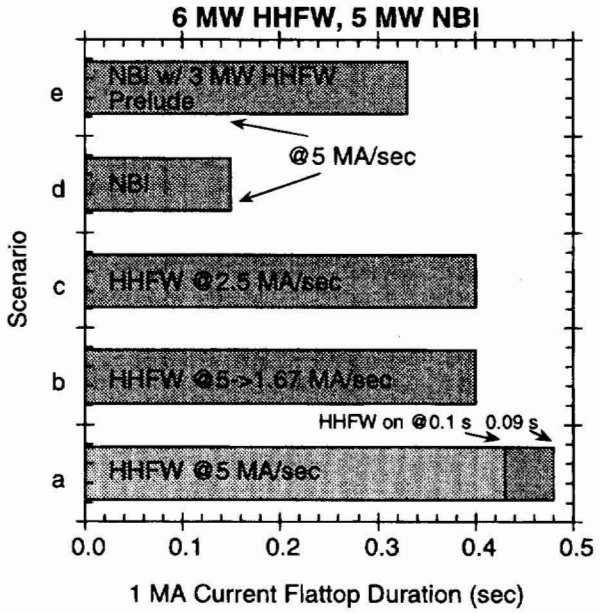

Fig. 13. Shown are 1-MA current flattop durations for inductive discharges under different heating scenarios.

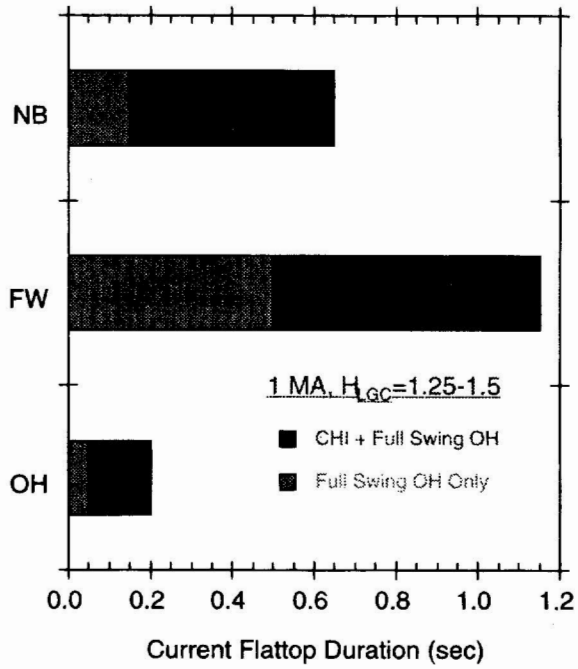

Fig. 14. Shown are 1-MA current flattop durations for a variety of heating scenarios with and without a 0.5-MA target plasma produced by CHI.

TABLE III

Expected Plasma Performance for Different Heating Scenarios

Scenario	$\bar{n}_e$ 10^{19} m^{-3}	$T_e(0)$ (keV)	$T_i(0)$ (keV)
OH	2.4	0.7	0.7
5-MW NBI	4.7	1.7	2.7
6-MW HHFW	3.7	4.0	1.6

was based on the NB deposition profile shape that was calculated in the TRANSP Monte Carlo code. This profile was peaked on-axis.

In the simulations discussed earlier, the bulk of the plasma current was driven by inductive means. Fully noninductive operation with pulse lengths greater than the current relaxation time is one of the objectives of NSTX. Accordingly, a simulation for a discharge duration of ~5 s was carried out to determine the key elements necessary for producing a noninductive discharge and to define the maximum pulse length required for NSTX. For this simulation, twice ITER97L confinement was assumed, and the CHI was assumed to produce a fully elongated, 0.5-MA target plasma with a relatively flat current

profile ($q_0 \sim 3$, $q_\psi \sim 10$). Fast-wave power of 2 MW was then applied, increasing to 6 MW over the course of 0.6 s. Accompanying this was a fast-wave-driven current of 0.4 MA. The current drive profile was initially peaked on-axis, but then the fraction of on-axis current drive was reduced essentially to zero 1.4 s later, consistent with the PICES calculations of the driven current profile for these plasma conditions. Augmenting this 0.4 MA of HHFW-driven current was 0.6 MA of bootstrap current drive, the two mechanisms accounting for most of the full 1 MA of plasma current during this phase. The β_t increased, reaching the 40% level 1.5 s into the simulation and remaining constant thereafter.

The toroidal current density profile relaxation is shown in Fig. 15. This figure contains snapshots of current profiles from various time periods during the discharge. The profile starts out relatively flat at 0.2 s (the start of the simulation), except for the toroidal effects causing the current density on the inside to be greater than that on the outside, consistent with CHI startup. As HHFW current drive and heating is applied and as the bootstrap current builds up, the current profile becomes hollow, with very low current density in the center due to flux exclusion from trying to drive current there. As the current drive in the central region is reduced, the profile readjusts, but it does not come to a steady state until 2 to 4 s into the discharge. This current relaxation time, which is consistent with the simple estimate presented earlier in the paper, defines the pulse length specification of 5 s. Despite the hollowness of the current profile, the q-profile, which relaxes on the same timescale as that of the current, remains essentially monotonic, with a broad low-shear region across the inner portion of the plasma.

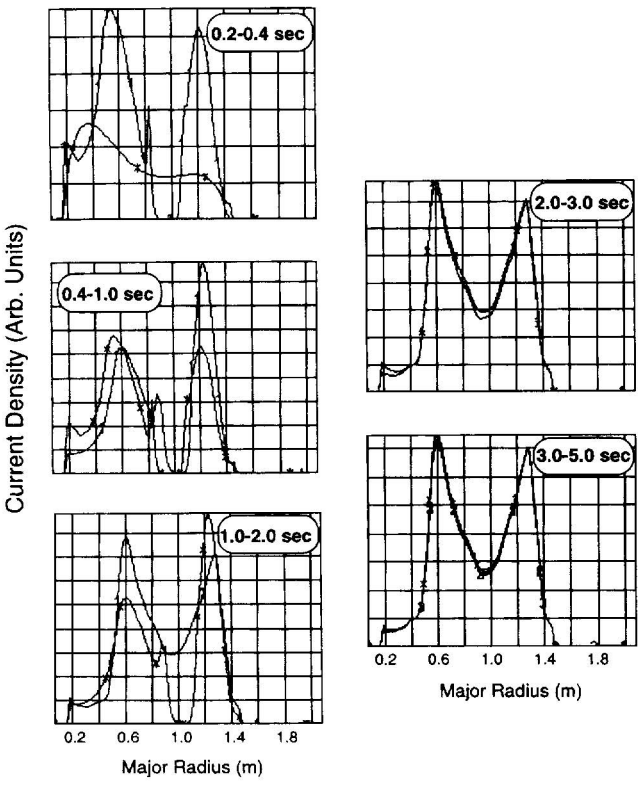

Fig. 15. Evolution of current density during noninductive discharge simulation.

V.E. Power and Particle Handling

NSTX is designed to produce distinctly different divertor and limiter configurations (Fig. 2): double and single nulls, where the plasma is defined by a separatrix and X points within the vessel, and a "natural" inner-wall-limited configuration, where the outboard SOL is diverted without any X points at the plasma edge. This capability will permit divertor physics tests of critical importance to future compact ST fusion cores of high power density. The divertor strike plates and plasma-facing components must be designed to handle adequately the expected maximum heat fluxes for all configurations for discharge durations of at least several seconds.

In OH-only plasmas, the maximum heating power is expected to be ~1.5 MW for a current flattop duration of up to several hundred milliseconds. Such plasmas are not expected to introduce the maximum heat fluxes for NSTX. In auxiliary-heated discharges, the baseline design maximum power is 6 MW for a pulse length of 5 s (P/R = 7.2 MW/m, P/A_{sep} = 0.2 MW/m^2). NBI could add another 5 MW of injected power. The peak heat flux to the divertor and center stack tiles has been estimated by simple power balance considerations and corroborated with analytic and two-dimensional numerical modeling. The peak heat flux in the divertor can be estimated by assuming an exponential heat flux profile in both the divertor and the midplane and by relating the divertor SOL power flux width to that in the midplane by geometry and flux expansion; i.e., $\lambda_q^{sol} = \lambda_q^{mid} f_{exp}/\sin(\alpha)$, where f_{exp} is the poloidal flux expansion from the midplane to the target at the 1-cm flux line and α is the angle of the separatrix and the target in the poloidal plane, measured from the horizontal direction. Power balance requires that

$$P_{target} = q_{peak}^{div}(\lambda_q^{sol} - \lambda_q^{pfr}) 2\pi R_{osp} \ , \qquad (11)$$

where P_{target} is the divertor target power, λ_q^{pfr} is the SOL heat flux width in the private-flux region, λ_q^{div} is that at the target, and R_{osp} is the outer strike point radius. In addition, the divertor target power is related to the heating power P_{heat} by

$$P_{target} = P_{heat} f_{out}(1 - f_{rad})/N_{div} \ , \qquad (12)$$

where f_{out} is the ratio of power flow in the outer divertor side to the total power flow into the SOL, f_{rad} is the radiated power fraction, and N_{div} is the number of divertors (equally) sharing the power. Substituting for λ_q^{sol} and P_{target} in Eq. (11) yields

$$q_{peak}^{div} = P_{heat} f_{out}(1 - f_{rad})\sin(\alpha) \times N_{div} \lambda_q^{mid} f_{exp}\left(1 + \frac{\lambda_q^{pfr}}{\lambda_q^{sol}}\right) 2\pi R_{osp} \ . \quad (13)$$

Several of the quantities in Eqs. (12) and (13) can be estimated from measurements made on other tokamaks; the remainder are geometry dependent. In the initial NSTX operational phase, a maximum P_{heat} of 6 MW is anticipated; also, $N_{div} = 2$. Based on observations from DIII-D double-null discharges,[36] $f_{out} = 0.8$, $f_{rad} = 0.3$, and $\lambda_q^{pfr}/\lambda_q^{div} = 0.33$ are used. Finally, λ_q^{mid} is estimated as 1 cm, as observed in DIII-D and other tokamaks.[37] The geometric quantities R_{osp}, f_{exp}, and α are equilibrium dependent. Four equilibria are considered: $l_i = 0.2$ and 0.6, the double-null divertor (DND), and IWL. For the IWL configurations, the P_{target} is reduced by an additional 20% to account for power deposition on the center stack. As shown in Table IV, the highest heat flux is observed in the $l_i = 0.2$ DND, due primarily to the low-flux expansion.

The largest potential uncertainty in this peak heat flux estimate is the assumed λ_q^{mid}. To corroborate this assumption, the Borass two-point model[38] of the SOL and divertor was applied to NSTX (Ref. 39). This model uses Bohm diffusion for the radial particle and energy transport rates; $\lambda_q^{mid} \sim 1.2$ cm is predicted for the NSTX parameters listed earlier. Finally, two-dimensional numerical calculations with the b2.5 edge plasma transport code[40] using Bohm radial transport rates predicted a similar λ_q^{mid} and peak heat flux for NSTX (Ref. 41).

The peak heat flux to the center stack $q_{peak,cs}$ is given by

$$q_{peak,cs} = P_{heat}(1 - f_{rad}) f_{iwl} f_{peak} / 4\pi R_{cs} h \ , \quad (14)$$

where

f_{iwl} = fraction of power flow to the inner wall

f_{peak} = profile-peaking factor

R_{cs} = center stack radius

h = center stack height.

TABLE IV

Summary of 0-D Heat Flux Calculations

Equilibrium	R_{osp} (m)	f_{exp}	α (deg)	q_{peak} (MW/m^2)
$l_i = 0.2$ DND	0.79	2.5	60	7.2
$l_i = 0.6$ DND	0.79	5	45	4.4
$l_i = 0.2$ IWL	0.60	5	45	3.8
$l_i = 0.6$ IWL	0.60	10	45	2.1

Note that f_{peak} is needed in this case because Eq. (14) yields the average heat flux for the center stack. DIII-D experiments in marginally IWL configurations have measured up to one-half of the nonradiated power fraction incident on the inner wall ($f_{iwl} \leq 0.5$) (Ref. 42). As a conservative design, we assume $f_{iwl} = 0.6$ and also that $f_{peak} = 2$. In addition, $R_{cs} = 0.185$ m and $h = 1.2$ m. As in the divertor calculations, $P_{heat} = 6$ MW and $f_{rad} = 0.3$. This yields a $q_{peak,cs} \simeq 2$ MW/m^2.

The thermal constraint on the divertor and center stack graphite tiles is 1200°C, which leaves a 200°C safety margin before radiation-enhanced sublimation would result in carbon blooms. One-dimensional and two-dimensional time-dependent calculations with the tile engineering design were done to determine the tile thermal response to a heat flux for the full-discharge duration of 5 s, followed by a cooldown time between discharges of 300 s. The thermal response calculations indicated that the highest computed peak heat flux of 7.2 MW/m^2, which occurs in the divertor, would result in a tile temperature marginally above the constraint (T_{max} = 1200°C). However, this peak temperature would be easily reduced by strike point sweeping, which is within the design capability of the PF coil set, or by nominal gas injection during discharges. The active divertor cooling between pulses will prevent ratcheting of the tile temperature over the course of the day.

Two-dimensional calculations of the center stack tiles exposed to a peak heat flux of 2 MW/m^2 indicate a peak tile temperature of $\leq$1000°C after several discharges (the center stack tiles are not actively cooled, and thus they are expected to ratchet up during the course of a day). Consequently, the center stack tiles have more safety margin than the divertor tiles with regard to thermal response, but both are expected to be acceptable for the baseline IWL or DND discharge configurations. Additional heating power or single-null operation will require aggressive heat-flux-reduction techniques and/or reduction in discharge pulse length.

VI. DIAGNOSTICS

The purpose of plasma diagnostics is to provide information on discharge parameters to characterize NSTX plasmas and to guide NSTX operations for optimized performance. The near-term emphasis will be on diagnostics in support of initial NSTX operation, but very shortly thereafter the focus will shift to understanding the basic confinement and transport properties of ohmically heated NSTX discharges. A list of the baseline diagnostics and their purpose is given in Table V.

The long-term objective is to upgrade and expand the diagnostic set for the study of fluctuations, transport, and MHD, both in the core and at the edge, in high-performance NSTX plasmas. Because of the need

TABLE V

Baseline Diagnostics

Diagnostic	Measurement
Plasma current Rogowski coils	Total plasma current
Eddy current Rogowski coils	Halo current monitoring
Flux loops	Poloidal flux for plasma control
B_θ, B_ρ coils	Magnetic field for control and fluctuations
Mirnov coils	Magnetic fluctuations
Visible television camera	Plasma position and shape for control
Infrared camera	Heat loads
Diamagnetic loop (TF coil)	Stored energy
Multichannel bolometer	Radiated power profile
170-GHz μwave interferometer	Line-integrated plasma density
Survey spectrometer (SPRED)	Impurities
Visible spectrometer	Edge/divertor spectroscopy
Visible bremsstrahlung	Z_{eff} profile
Soft X-ray imaging	Internal fluctuations, plasma equilibrium
D_α detectors	Edge recycling
CHERS	Ion temperature profile and toroidal rotation
X-ray pulse-height analyzer	Core electron temperature
Neutral particle analyzer	Core ion temperature and fast ions
Ultrasoft X-ray array	Startup and impurity studies
Langmuir probes/thermocouples	Divertor parameters

for profile measurements to study the transport processes in NSTX plasmas, high priority will be placed on having a multipulse Thomson scattering diagnostic available shortly after initial operation. In addition, special emphasis will be placed on developing and installing current profile measurements because of their particular importance. Although there are special challenges for a Motional Stark Effect diagnostic at the low B_T of NSTX, the plan is to have some variant of this technique at the time the NB system is brought on line. A list of some of the potential upgrade diagnostics is given in Table VI. New concepts and additional systems developed by the national NSTX team to achieve the project goals also will be encouraged.

VII. RESEARCH PLAN

The proposed NSTX research plan during the first several years of operation naturally divides into three distinct phases. The first phase of operation, to be conducted after the April 1999 first plasma and a component shakedown period, is the study of startup and ohmic/low power plasmas. The goals of this phase are as follows:

1. to explore and establish operational space
2. to characterize OH/low power confinement and operational limits
3. to test and develop HHFW heating scenarios
4. to test and develop CHI current initiation.

The approaches to achieving these goals include inductive operation with EC preionization, vessel and tile conditioning, baseline diagnostics and the multipulse Thomson scattering system, and a rudimentary plasma position control system. It is anticipated that, during this period, HHFW powers of up to 4 MW will be injected into the plasma, and currents up to 1 MA with current flattop durations of up to 0.5 s will be attained. It is expected that this phase will last ~1 yr.

Phase II will focus on the heating and noninductive operations for startup and moderate β_t. The goals of this phase are

1. to establish CHI noninductive startup techniques
2. to establish confinement scalings of ST plasmas heated to moderate β_t
3. to study local transport and turbulence properties, including transport barrier formation
4. to study the approach to β_t limits at moderate β_t
5. to investigate SOL properties for diverted and IWL configurations
6. to explore and characterize current drive during the current sustainment phase (HHFW, CHI, and bootstrap).

TABLE VI

Upgrade Diagnostics

Diagnostic	Measurement
Multipulse Thomson scattering	Electron temperature and density profiles
Motional Stark Effect	Current profile
Tangential X-ray imaging	Internal fluctuations
Fission chambers	Fusion products
Fast neutron detectors	MHD activity
Fast ion loss probes	Fast ion loss distribution
Far-infrared scattering	Fluctuations
Laser-enhanced beam emission spectroscopy	Fluctuations
Atomic beam emission	Edge fluctuations
Fast edge imaging	Edge fluctuations
Poloidal CHERS	Poloidal rotation
Fast reciprocating edge probe	Edge temperature and density
Tangential interferometer/polarimeter	Density and toroidal field profiles
Edge interferometer	Density profile
Heavy ion beam probe	Plasma potential and current distributions
Divertor bolometers	Radiated power in divertor
Divertor SPRED	Divertor impurities
Divertor Thomson scattering	Divertor temperature and density profiles

During this phase, the full 6 MW of HHFW will be injected into the plasma, and the 5-MW neutral beam will be brought on line, the latter enabling the use of NBI-based diagnostics such as MSE and CHERS. Along with these diagnostics, other profile and turbulence diagnostics, as well as SOL and plasma-surface interaction diagnostics, will be employed. As mentioned, both OH and noninductive current-drive techniques will be used, as will density control techniques, to achieve high-confinement, high-β_t operation. Aspect ratio scans will be performed to connect the results to those at conventional aspect ratio. The plasmas produced during this phase are expected to have current flattop durations of up to 1 s, and they are expected to be in the first stability regime ($q_0 \simeq 1$, $\beta_t \leq 25\%$). This phase, in the success-oriented schedule, should last for $\sim$1.5 yr.

The third and final phase of operation for the initial NSTX configuration is the advanced physics regime, in which the various tools will be employed to produce and maintain high-performance plasmas. The goals for this phase are

1. to achieve fully noninductive startup and current sustainment at high power for several seconds
2. to achieve control of the edge and core transport barriers for good confinement
3. to achieve and maintain high β_t
4. to investigate the unique features in an ST plasma edge and SOL.

Current profile control will be achieved through the various heating and current-drive systems (including a well-aligned bootstrap current) and active transport barrier control through pressure profile control, and advanced core and edge diagnostics will be employed. During this phase, in which the plasmas may be in the second stability regime, β_t values of up to 40% and self-drive (i.e., bootstrap) current fractions of up to 70% for pulse lengths of up to 5 s are the targets. This phase may last for several years.

VIII. PHYSICS SUMMARY

The physics investigations discussed earlier indicate the promise of NSTX in fulfilling its mission objectives to study the basic plasma and fusion-related science of low-aspect-ratio configurations and to demonstrate the viability of STs in reactor-relevant regimes. In particular, NSTX addresses directly the key areas of shaping and configurational flexibility, confinement and transport, MHD stability, noninductive current drive, and power handling. Operational scenarios, both inductive and noninductive, are being developed, which give guidance on the effects of the various heating and current-drive systems and how various combinations of these techniques will be required for NSTX to achieve its goals.

Specific science issues to be addressed include global confinement properties of ST plasmas at low collisionality and the suppression of electrostatic and electromagnetic turbulence. Such suppression is expected as the

aspect ratio is reduced due to an increase in orbit-averaged good curvature and the low shear on the inboard side of the plasma as the aspect ratio decreases. This suppression is expected to be aided by the high rotational shearing rate due, primarily, to the low toroidal field at low aspect ratio. Furthermore, high-β_t ST configurations, such as the ones to be produced in NSTX, carve out a magnetic well near the magnetic axis, reducing the proportion of trapped particles there and, thus, reducing the instability drive for kinetically driven modes.

NSTX will study the ballooning and kink stability at low aspect ratio and their dependence on variations in aspect ratio, shaping, and the presence of the conducting plates, with an aim of producing high-β_t (25 to 40%) configurations. The role of resistive wall modes and Alfvén eigenmodes at low aspect ratio will be addressed. Operation at high q, high β_t, and low collisionality is a prerequisite for high-bootstrap and thus fully noninductive operation. NSTX will also determine the lower q limit for stable, disruption-free operation.

Since plasma pressure and current profile control are important for producing the high-β_t, high-bootstrap configuration, NSTX will employ various means to achieve this goal. Specifically, HHFW will be used to heat the plasma and to drive the current and control the current profile (in the core region at low β_t and farther out at high β_t). HHFW is well suited to ST operation because of its strong single-pass absorption and predominant electron heating. CHI will be tested for discharge startup and for current drive in the outer portion of the plasma during the current sustainment phase.

Important issues in the area of power and particle handling are SOL characterization and the physics that drives transport there. Furthermore, because of its built-in shape and configurational flexibility, NSTX will investigate the effect of varying configurations and control schemes to reduce divertor heat loads.

ACKNOWLEDGMENTS

This work was supported by the U.S. Department of Energy under the following contracts: DE-AC02-CHO3073 at the Princeton Plasma Physics Laboratory, DE-FG02-89ER53297 at Columbia University, DE-AC05-96OR22464 at Oak Ridge National Laboratory, and DE-FG06-90ER54095 at the University of Washington.

REFERENCES

1. GATES et al., *Phys. Plasmas*, **5**, 1775 (1998).

2. ONO et al., "Investigation of the Effect of Resistive MHD Modes on Spherical Torus Performance in CDX-U," *Proc. 16th Int. Conf. Plasma Physics and Controlled Nuclear Fusion Research*, Montreal, Canada, October 7–11, 1996; see also *Fusion Energy 1996*, Vol. 2, p. 71, International Atomic Energy Agency (1997).

3. T. JARBOE et al., "Recent Results of the Helicity Injected Tokamak Experiment," *Proc. 16th Int. Conf. Plasma Physics and Controlled Nuclear Fusion Research*, Montreal, Canada, October 7–11, 1996; see also *Fusion Energy 1996*, Vol. 2, p. 243, International Atomic Energy Agency (1997).

4. J. MENARD et al., *Nucl. Fusion*, **37**, 595 (1997).

5. G. REWOLDT et al., *Phys. Plasmas*, **3**, 1 (1996).

6. R. STAMBAUGH et al., "The Spherical Torus Approach to Magnetic Fusion Development," *Proc. 16th Int. Conf. Plasma Physics and Controlled Nuclear Fusion Research*, Montreal, Canada, October 7–11, 1996; see also *Fusion Energy 1996*, Vol. 2, p. 395, International Atomic Energy Agency (1997).

7. R. BUTTERY et al., "Steady State Spherical Tokamaks and Future Applications," *Plasma Physics Continuing Nuclear Fusion Research*, Vol. 2, p. 633, International Atomic Energy Agency (1995).

8. M. PENG et al., "Physics Progress Towards Compact Tokamak Reactors with Normal Conducting Toroidal Field Coils, *Proc. 15th Int. Conf. Plasma Physics and Controlled Nuclear Fusion Research*, Madrid, Spain, September 26–October 1, 1994; see also *Plasma Physics Continuing Nuclear Fusion Research*, Vol. 2, p. 643, International Atomic Energy Agency (1995).

9. M. PENG and D. STRICKLER, *Nucl. Fusion*, **26**, 769 (1986).

10. M. O'BRIEN et al., "Stability and Additional Heating Properties of Spherical Tokamak Plasmas on START," *Proc. 16th Int. Conf. Plasma Physics and Controlled Nuclear Fusion Research*, Montreal, Canada, October 7–11, 1996; see also *Fusion Energy 1996*, Vol. 2, p. 57, International Atomic Energy Agency (1997).

11. P. YUSHMANOV et al., *Nucl. Fusion*, **30**, 1999 (1990).

12. D. P. SCHISSEL and the ITER H-Mode Confinement Working Group, "Analysis of the ITER H-Mode Confinement Database," *Proc. 20th European Conf. Controlled Fusion and Plasma Physics*, Lisbon, Portugal, July 26–30, 1993; see also *Controlled Fusion and Plasma Physics*, Vol. 17C, p. 103, European Physical Society (1993).

13. S. M. KAYE and the ITER Confinement Database Working Group, *Nucl. Fusion*, **37**, 1303 (1997).

14. M. ROBERTO and R. GALVAO, *Nucl. Fusion*, **32**, 1666 (1982).

15. R. GALVAO, S. KALMYKOV, M. ROBERTO, and W. DESA, *Comments Plasma Phys. Controll. Fusion*, **15**, 219 (1993).

16. R. AKERS et al., "Ion Physics in the START Spherical Tokamak," *Proc. 25th Conf. Controlled Fusion and Plasma Physics*, Prague, Czech Republic, June 29–July 3, 1998; see

also *Controlled Fusion and Plasma Physics*, European Physical Society (to be published).

17. S. KAYE et al., *Nucl. Fusion*, **28**, 1963 (1988).

18. M. OKABAYASHI et al., *Nucl. Fusion*, **36**, 1167 (1996).

19. E. LAZARUS et al., "The Role of Shaping in Achieving High Performance in DIII-D, *Proc. 15th Int. Conf. Plasma Physics and Controlled Nuclear Fusion Research*, Madrid, Spain, September 26–October 1, 1994; see also *Plasma Physics Continuing Nuclear Fusion Research*, Vol. 1, p. 609, International Atomic Energy Agency (1995).

20. M. ONO, *Phys. Plasmas*, **2**, 4075 (1995).

21. D. MIKKELSEN, *Phys. Fluids B*, **1**, 333 (1989).

22. K. LACKNER and N. GOTTARDI, *Nucl. Fusion*, **30**, 767 (1990).

23. A. SYKES et al., "Tight Aspect Ratio Tokamak Experiments and Prospects for the Future," *Proc. Int. Conf. Plasma Physics ICPP1994*, Woodbury, New York, 1995, p. 110; see also Conf. Proc. 345, American Institute of Physics.

24. F. RYTER and the ITER H-Mode Database Working Group, "Plasma Physics Control," *Fusion*, **38**, 1279 (1996).

25. T. HAHM and K. BURRELL, *Phys. Plasmas*, **2**, 1648 (1995).

26. D. WARD, A. BONDESON, and F. HOFMANN, *Nucl. Fusion*, **33**, 821 (1993).

27. C. KESSEL, S. JARDIN, and G. NEILSON, "Plasma Vertical Stability and Feedback Control for TPX," presented at 15th Int. Symp. Fusion Engineering, Hyannis, Massachusetts, October 11–15, 1993; see also IEEE 93CH3348-0, Institute of Electrical and Electronics Engineers (1994).

28. J. RICE et al., *Nucl. Fusion*, **38**, 75 (1998).

29. G. NAVARTIL et al., *Phys. Plasmas*, **5**, 1855 (1998).

30. M. CARTER et al., *Nucl. Fusion*, **36**, 209 (1996).

31. F. JAEGER et al., *Nucl. Fusion*, **33**, 179 (1993).

32. D. EHST and C. KARNEY, *Nucl. Fusion*, **32**, 1933 (1991).

33. S. JARDIN et al., *J. Comp. Phys.*, **66**, 481 (1986).

34. S. JARDIN et al., *Nucl. Fusion*, **33**, 371 (1993).

35. W. TANG et al., *Nucl. Fusion*, **26**, 1605 (1986).

36. T. PETRIE et al., "The Role of Neutrals in the H-L Back Transition of High Density Single-Null and Double-Null Gas Fueled Discharges in DIII-D," *J. Nucl. Mater.* (1998).

37. C. LASNIER et al., "Survey of Target Plate Heat Flux in Diverted DIII-D Tokamak Discharges," *Nucl. Fusion* (1998).

38. K. BORASS, *Nucl. Fusion*, **31**, 1035 (1991).

39. R. MAINGI, "Edge Plasma Modeling in STs," *Proc. Int. Workshop STs*, Abingdon, United Kingdom, 1996.

40. B. BRAAMS, *Contributions to Plasma Physics*, **36**, 276 (1996).

41. R. MAINGI, "2-D Edge Plasma Transport Calculations for NSTX," *Proc. Int. Workshop STs*, St. Petersburg, Russia, 1997.

42. G. JACKSON et al., *Plasma Phys.*, **3**, 1005 (1996).

Stanley M. Kaye [BA, physics and math, Hamilton College, 1974; M.Sc., geophysics and space physics, University of Washington, 1976; PhD, earth and space sciences, University of California, Los Angeles (UCLA), 1979] is head of the Physics Analysis Division, National Spherical Torus Experiment (NSTX). His interests include spherical tori, confinement and transport, magnetohydrodynamics (MHDs), plasma startup, data management, and database tools.

Masayuki Ono [BS, physics, California Institute of Technology (Caltech), 1973; PhD, plasma physics, Princeton University, 1978] is the NSTX project director. His interests include spherical tori, high-beta plasmas, plasma startup and heating, and current drive.

Yueng-Kay Martin Peng (BS, electrical engineering, National Taiwan University, 1967; PhD, applied physics, Stanford University, 1974) is program director of NSTX. His interests include properties of high-temperature spherical torus plasmas and implications for fusion energy development.

Donald B. Batchelor [BS, physics, Massachusetts Institute of Technology (MIT), 1968; PhD, physics, University of Maryland, 1976] is head of the Plasma Theory Section at Oak Ridge National Laboratory (ORNL). His interests include wave/plasma interactions, at frequencies ranging from ion cyclotron resonance frequency to electron cyclotron heating, and compact stellarator design.

Mark D. Carter (BS, nuclear engineering, University of Missouri, Rolla, 1980; PhD, nuclear engineering, University of Wisconsin-Madison, 1985) is on the research staff at ORNL. His interests include radio frequency (rf) design and analysis for plasma applications, plasma thrusters, and rf/edge interactions in fusion experiments.

Wonho Choe (BS, nuclear engineering, Seoul National University, Korea, 1985; PhD, plasma physics, Princeton University, 1996) is an assistant professor at the Korea Advanced Institute of Science and Technology, Korea. His interests include tokamak plasma physics, plasma diagnostics, and dusty plasmas.

Robert Goldston (BS, physics, Harvard University, 1972; PhD, astrophysical sciences, Princeton University, 1977) is director of the Princeton Plasma Physics Laboratory (PPPL). His interests include developing and implementing innovative ideas to make fusion practical.

Yong-Seok Hwang (BS, 1983, and MS, 1986, nuclear engineering, Seoul National University, Korea; PhD, plasma physics, Princeton University, 1992) is an assistant professor in the Nuclear Engineering Department at Seoul National University. His interests include plasma control and plasma source development.

E. Fred Jaeger (BS, nuclear engineering, Columbia University, 1966; PhD, nuclear engineering, University of California, Berkeley, 1970) is a senior research staff member at ORNL. His interests include computational plasma physics and developing two- and three-dimensional models for ion cyclotron wave propagation, absorption, and current drive in high-temperature plasmas.

Thomas R. Jarboe (BS, University of Illinois, 1967; PhD, University of California, Berkeley, 1974) is a professor of aeronautics and astronautics and an adjunct professor of physics at the University of Washington. His interests include helicity injection current drive and associated physics.

Stephen Jardin (BS, engineering physics, University of California, Berkeley, 1970; MS, nuclear engineering and physics, MIT, 1973; PhD, plasma physics, Princeton University, 1976) is deputy head of the Theory Department at PPPL. His interests include computational MHD applied to magnetic fusion plasmas.

David Johnson (BA, physics and math, St. Olaf College, 1970; PhD, physics, Harvard University) is head of the Diagnostics Development Division at PPPL. His interests include development of new instrumentation to diagnose plasma properties.

Robert Kaita (BS, physics, State University of New York, Stoneybrook, 1973; PhD, nuclear physics, Rutgers University, 1978) is cohead of the Current Drive Experiment-Upgrade (CDX-U) at PPPL and head of NSTX diagnostics. His interests include high-temperature plasma diagnostics, physics of plasma heating, and MHD instabilities.

Charles Kessel (BS, physics, University of California, Santa Barbara, 1982; PhD, fusion engineering and applied plasma physics, UCLA, 1987) is a senior engineer at PPPL. His interests include plasma equilibrium and stability, plasma engineering, and dynamic plasma simulation and control.

Henry Kugel is a principal research physicist at PPPL. He is coordinating the research and development and the installation of in-vessel sensors and edge diagnostics for NSTX. His current research interests include the physics of the plasma edge.

Rajesh Maingi (BS, 1987, and PhD, 1992, nuclear engineering, North Carolina State University) is a research scientist with Lockheed Martin Energy Research Corporation. His interests include boundary physics experiments and modeling.

Richard Majeski (BS, 1973, and MS, 1974, physics, University of Scranton; PhD, physics, Dartmouth College, 1979) is head of CDX-U at PPPL. His interests include rf heating and current drive and pressure profile control in fusion plasmas.

Janhardan Manickam (BS, physics, math, and chemistry, Osmania University, India, 1966; MS, nuclear physics, Andhra University, India, 1968; PhD,

plasma physics, Stevens Institute of Technology, 1975) is a principal research physicist at PPPL. His interests include theory and interpretation of MHD stability in tokamaks and reactor design.

Jonathan Menard (BS, nuclear engineering, University of Wisconsin–Madison, 1992; PhD, plasma physics, Princeton University, 1998) is an associate research physicist at PPPL. His interests include MHD stability limits of spherical torus plasmas, fast wave heating, and current drive in spherical torus plasmas.

David R. Mikkelsen (BS, Caltech, 1971; PhD, University of Washington, 1975) is a research physicist at PPPL. His interests include computer simulation of tokamak thermal transport, neutral beam injection, and energetic ion orbits.

David J. Orvis (BS, physics, Harvey Mudd College, 1990; MS, nuclear engineering, 1993, and MS, applied math, 1995, University of Washington; PhD, nuclear engineering, University of Washington, 1997) is a software engineer testing and developing software for the Windows CE operating system.

Brian A. Nelson (BSEE, University of Iowa, 1981; MSNE, 1983, and PhD, nuclear engineering–engineering physics, 1987, University of Wisconsin-Madison) is a research-associate professor at the University of Washington, where he is a coprincipal investigator on the Helicity Injected Torus and ZaP Z-pinch experiments. His interests include fusion plasmas, magnetic helicity, and inductive plasma sources.

Franco Paoletti (PhD, physics, University of Rome, Italy, 1989) is an associate research scientist at Columbia University. His interests include magnetic equilibrium, ideal MHD, and rf application to magnetic confinement devices.

Neil Pomphrey (BS, chemical physics, Edinburgh University, Scotland; PhD, physics, Stirling University, Scotland, 1975) is a principal research physicist with interest in MHD.

Gregory Rewoldt (BS, physics, Caltech, 1970; PhD, physics, MIT, 1974) is a principal research physicist at PPPL. His interests include theoretical plasma physics, and specifically linear microinstability theory in tokamaks and stellarators.

Steven Sabbagh (BS, 1984, and PhD, 1990, applied physics, Columbia University) is a research scientist at Columbia University. His interests include computational physics, MHD equilibrium and stability, and magnetic fusion experiments.

Dennis J. Strickler (BS, mathematics, Berea College, 1971; MA, mathematics, University of Kentucky, 1973) is a staff member in Computational Physics and Engineering at ORNL. His interests include MHD equilibrium and plasma control, and poloidal field coil design.

Edmund Synakowski (BA, physics, Johns Hopkins University, 1982; PhD, physics, University of Texas at Austin, 1988) is a principal research physicist at PPPL. His interests include plasma confinement bifurcations, transport modification through $E \times B$ flow shear effects, plasma spectroscopy, helium transport, and ash measurements.

James R. Wilson (BS, physics, University of Michigan, 1974; PhD, astrophysical sciences, Princeton University, 1980) is a principal research physicist at PPPL. His interests include heating and current drive, stability of fusion plasmas, and wave propagation, absorption, and instabilities in plasmas.